





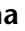







Efficient oxidation attenuates porewater-derived methane fluxes in mangrove waters

Yvonne Y. Y. Yau ^{1*}, Alex Cabral ¹, Gloria Reithmaier ¹, Luiz C. Cotovicz Jr ^{2,3}, João Barreira ⁴,
Gwenaél Abril ^{4,5}, Cedric Morana ⁶, Alberto V. Borges ⁶, Wilson Machado ⁴, José M. Godoy ⁷,
Stefano Bonaglia ¹, Isaac R. Santos ¹

¹Department of Marine Sciences, University of Gothenburg, Gothenburg, Sweden

²Department of Marine Chemistry, Leibniz Institute for Baltic Sea Research, Warnemünde, Germany

³Centro de Estudos do Mar, Universidade Federal do Paraná, Pontal do Paraná, Brazil

⁴Department of Geochemistry, Fluminense Federal University, Niterói, Brazil

⁵Laboratoire de Biologie des Organismes et Ecosystèmes Aquatiques (BOREA), UMR 8067, Muséum National d'Histoire Naturelle, CNRS, IRD, SU, UA, Paris, France

⁶University of Liège, Chemical Oceanography Unit, Liège, Belgium

⁷Department of Chemistry, Pontifícia Catholic University of Rio de Janeiro, Gávea, Brazil

Abstract

Mangroves store significant amounts of carbon in both sediment and water. Methane (CH₄) is often produced in anoxic, organic-rich sediments during carbon degradation and released to overlying waters via porewater exchange. Yet, a portion of CH₄ can be oxidized to CO₂ before emission. Here, we investigate whether CH₄ oxidation impacts its emissions using high-temporal resolution CH₄ concentration and stable isotope (δ¹³C-CH₄) observations collected over 14 tidal cycles in 2 Brazilian mangrove creeks with no river inputs. We found higher CH₄ concentrations (~150 nM) more depleted in ¹³C (−75‰) during low tide than high tide at both creeks. Similar δ¹³C-CH₄ values between low tide surface waters and porewaters further suggest tidally driven porewater exchange as the main source of CH₄. More ¹³C-enriched CH₄ in surface waters and surface sediments than deep sediments indicate partial CH₄ oxidation prior to exchange with the atmosphere. A stable isotope mass balance revealed that 17–58% of CH₄ was oxidized at rates of 3–25 μmol m^{−2} d^{−1} in the water column of tidal creeks. A larger portion of deep porewater CH₄ (45–61%) was oxidized in sediments prior to porewater exchange with surface creek waters. The two mangrove creeks had average water–air CH₄ fluxes of 51–109 μmol m^{−2} d^{−1} over spring-neap tidal cycles. These aquatic CH₄ emissions offset only < 3% of the mangroves' soil carbon sequestration. Overall, CH₄ oxidation in both surface water and sediment attenuated CH₄ emissions to the atmosphere.

*Correspondence: yvonne.yau@gu.se

Additional Supporting Information may be found in the online version of this article.

This is an open access article under the terms of the [Creative Commons Attribution-NonCommercial](https://creativecommons.org/licenses/by-nc/4.0/) License, which permits use, distribution and reproduction in any medium, provided the original work is properly cited and is not used for commercial purposes.

Author Contribution Statement: YY: Investigation; Formal analysis; Visualization; Writing – original draft. AC: Investigation; Data analysis; Writing – review and editing. GR: Investigation; Conceptualization; Writing – review and editing. LC: Investigation; Conceptualization; Writing – review and editing. JR: Investigation; Writing – review and editing. GA: Conceptualization; Writing – review and editing. CM: Investigation; Methodology. AB: Conceptualization; Writing – review and editing. WM: Resources; Writing – review and editing. JG: Investigation. SB: Conceptualization; Resources; Writing – review and editing. IS: Investigation; Funding acquisition; Data curation; Review and editing; Supervision; Project administration; Writing – review and editing.

Mangroves at the land–ocean interface are known to sequester carbon through outwelling to coastal waters (Reithmaier et al. 2023) and burial of soil organic matter (Bouillon et al. 2008). However, this benefit is partially countered by emissions of methane (CH₄), a potent greenhouse gas. The abundance of organic matter in mangrove sediments, coupled with anoxic conditions provides ideal conditions for methanogenesis. A portion of the organic carbon in sediments is mineralized into CH₄, which can be released to the atmosphere or surrounding waters. CH₄ emissions from mangrove forests may offset 7–27% of the carbon sequestration in sediments (Cotovicz et al. 2024). Despite their importance in the marine carbon cycle and potential as a nature-based solution for mitigating climate change (Lovelock et al. 2022), CH₄ dynamics in mangroves remain poorly understood. Global estimates of CH₄ emissions (0.0684 Tg CH₄ yr^{−1}) from mangroves are highly uncertain (Cotovicz et al. 2024). Moreover,

factors influencing the CH₄ production, oxidation, and fluxes are poorly quantified across various spatial and temporal scales (Al-Haj and Fulweiler 2020; Rosentreter et al. 2021; Delwiche et al. 2021), which also bring uncertainties to global estimates.

Mangroves experience daily and weekly tidal cycles. Porewater exchange and seawater mixing influence redox conditions, biogeochemical properties, and ultimately, greenhouse gas production in sediments (Wang et al. 2020; Xin et al. 2022). While significant sediment–air CH₄ emissions have been measured in mangroves using chamber techniques (e.g., Chen et al. 2014; Castellón et al. 2022; Kristensen et al. 2022), the complex interaction between porewater, tides and water–air CH₄ emissions remains poorly understood (Barnes et al. 2006; Santos et al. 2019; Belliard et al. 2022; Cotovicz et al. 2024). Previous measurements in mangroves revealed that tidal forces exert a much greater influence on carbon cycling than seasonal dynamics (Jacotot et al. 2018; Call et al. 2019; Santos et al. 2019). Methanogenesis, the microbial production of CH₄, occurs in deep anoxic sediments through degradation of organic matter (Canfield et al. 2005; Taketani et al. 2010; Euler et al. 2023). Porewater thus becomes enriched in nutrients and greenhouse gases. Tidal fluctuations drive hydraulic gradients in sediments, potentially releasing gases from the sediments and exporting CH₄ to the atmosphere, nearby estuaries and the coastal ocean (Abril et al. 2013; Maher et al. 2018).

CH₄ emissions are a net balance of production and attenuation through oxidation (Le Mer and Roger 2001). Microbial processes within sediments oxidize CH₄ to carbon dioxide (CO₂) with the remaining CH₄ escaping to the overlying water column or the atmosphere (Hoehler et al. 1994; Reeburgh 2007). CH₄ can be consumed in the water column through aerobic oxidation. For example, CH₄ oxidation in lakes efficiently removes 30–99% of CH₄, usually in oxic waters and at the sediment–water interface (Bastviken et al. 2008). However, the magnitude of CH₄ oxidation in mangrove water columns remain poorly understood (Sánchez-Carrillo et al. 2021). Recent studies in Australian mangrove creeks suggested that CH₄ oxidation could reduce water–air CH₄ fluxes by 10–33% (Cotovicz et al. 2024). The drivers and magnitude of CH₄ oxidation along the path from sediment porewaters to the water column, particularly in mangroves with high carbon burial efficiency, are still unclear.

The stable carbon isotope ratios of CH₄ ($\delta^{13}\text{C-CH}_4$) provide a valuable tool to resolve the fate and oxidation rate of CH₄. When CH₄ undergoes oxidation, the residual CH₄ becomes enriched in the heavier carbon isotope (¹³C) because bacteria preferentially utilize the lighter isotope (¹²C) (Whiticar 1999; Holmes et al. 2015). Hence, the difference in $\delta^{13}\text{C-CH}_4$ between the sources and residual CH₄ can be used to quantify the fraction of CH₄ being oxidized if all CH₄ endmembers can be defined isotopically (Schenk et al. 2021). In deeper sediments where methanogenesis is particularly active, $\delta^{13}\text{C-CH}_4$ values can indicate dominant methanogenesis pathways.

Hydrogenotrophic methanogenesis and acetoclastic methanogenesis produce ¹³C depleted CH₄ with values from –65‰ to –50‰ and from –110‰ to –60‰, respectively (Whiticar 1999).

Here, we hypothesize that methane oxidation partially attenuates CH₄ emissions to the atmosphere from mangrove waters and sediments. We investigate CH₄ dynamics in mangroves focusing on both sources and oxidation rates within the water–air interface and sediment. We conducted detailed observations of CH₄ in sediments and creek waters capturing mangrove drainage at two sites in Brazil. We aim to (1) evaluate drivers of CH₄ water–air fluxes on daily and tidal time scales, (2) evaluate drivers and magnitude of CH₄ oxidation, and (3) quantify the global warming potential of water–air CH₄ fluxes compared to sediment carbon sequestration.

Methods

Study sites

The study was conducted in one tropical and one subtropical mangrove forest in Brazil (Fig. 1). The 1st mangrove creek (23°18'9.407''S, 44°38'58.92''W) is situated in the Paraty-Mirim National Park on the southern coast of Rio de Janeiro state (site M1). This is a well-preserved and pristine mangrove ecosystem away from any local sources of pollution within a nature reserve in the Saco do Mamanguá embayment (Barroso et al. 2022; Chynel et al. 2022) (Supporting Information Table S1). The creek is 1 km long, receives oligotrophic ocean waters at high tide, and exhibits negligible river influences (Brandini et al. 2019). The mangrove is dominated by *Avicennia schaueriana*. The average monthly temperature varied from 21°C to 28°C and monthly rainfall is 150 ± 94 mm. The mangrove creek experiences mixed semidiurnal tides with a tidal range of ~ 1.6 m. The 2nd mangrove creek (27°38'57.012''S, 48°33'10.92''W) is situated in a small reserve (Pirajubaé Marine Reserve) within the city of Florianópolis in South Brazil (site M2). The mangrove creek is influenced by sewage and industrial runoff from nearby urban areas (Cabral et al. 2020) (Supporting Information Table S1). The tidal regime is mixed semidiurnal with a tidal range of ~ 0.9 m. The average monthly temperature varied from 14°C to 27°C and monthly rainfall is 150 ± 94 mm. Both mangrove sites are located away from large river sources so that other inputs are expected to be small compared to biogeochemical processes within mangroves.

Surface water time series

Time series observations were conducted to resolve CH₄ dynamics in mangrove creeks at M1 from October 28, 2021 to November 4, 2021 and at M2 from November 27, 2021 to December 4, 2021. The time series captured 13–14 complete tidal cycles, spanning from neap to spring tide, representing the dominant time scale of variability within mangroves (Santos et al. 2019). A boat was stationed in the mouth of the

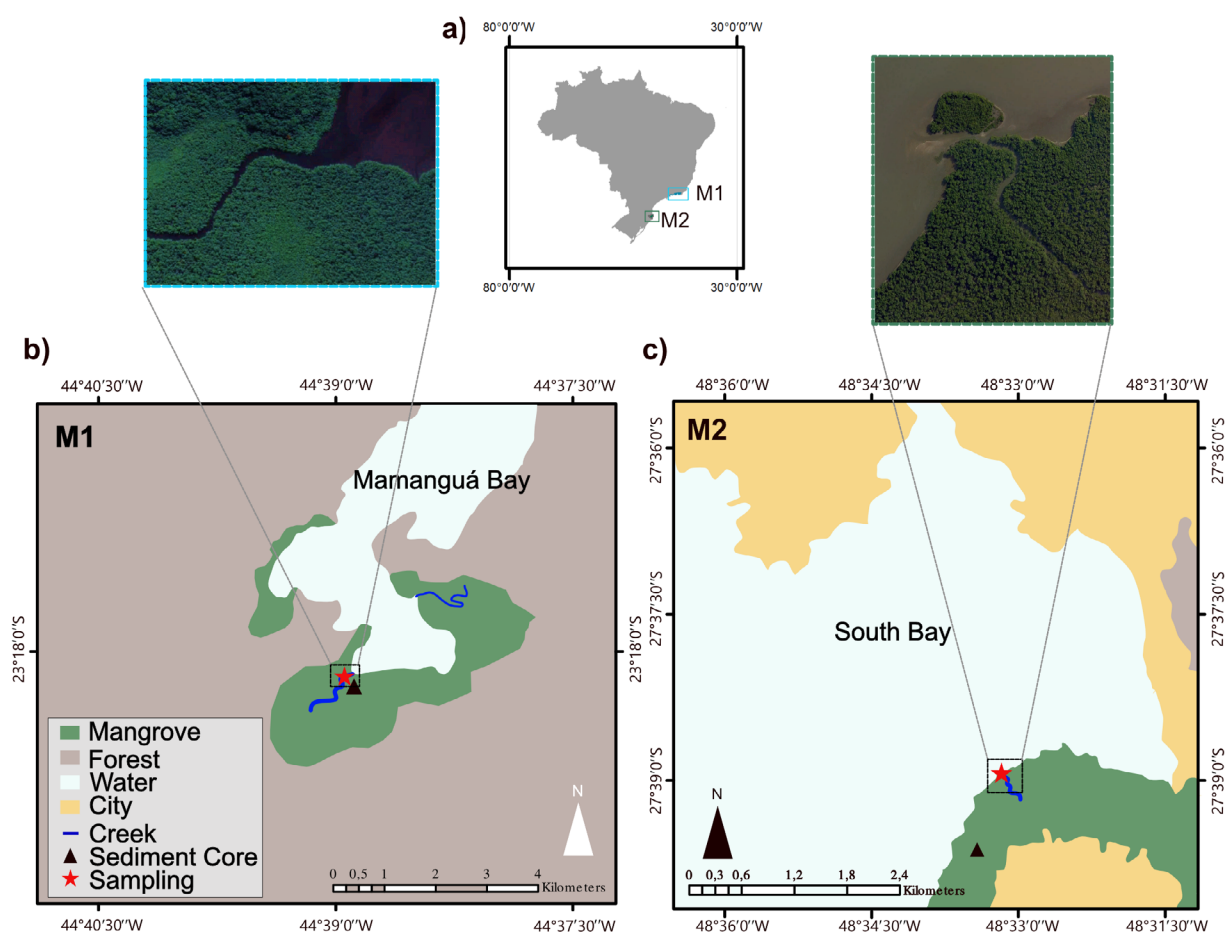


Fig. 1. Two mangrove sites were located in southeastern and southern Brazil (a). The study location of mangroves are (b) in the well-preserved Paraty-Mirim National Park (M1 site) and (c) the urban region around Florianópolis (M2 site). The red stars indicate the location of surface water time-series deployments, while triangles represent the location of sediment core and seep samples. The land use was extracted from Mapbiomas Project (MapBiomas Project 2024).

mangrove creek to set up a temporary time series station (Fig. 1). Surface water was continuously pumped through a showerhead gas equilibration device (RAD AQUA showerheads) connected to a radon (^{222}Rn) detector (RAD 7, Durridge) and a CH_4 gas analyzer (LI-7810, LI-COR). ^{222}Rn was determined at 30-min intervals, while CH_4 was recorded at 1-s intervals. Water depth, temperature, salinity (Levellogger 5 LTC, Solinst), and dissolved oxygen (DO, miniDOT, PME) were logged at 1 min time steps. Current velocity was measured using a bottom mounted acoustic doppler current profiler (ADCP, Nortek ECO). A lag of 30 min was used to correct the delayed response of CH_4 and ^{222}Rn when using this system (Webb et al. 2016).

To estimate CH_4 oxidation in waters, discrete surface water samples for CH_4 concentration, $\delta^{13}\text{C}-\text{CH}_4$ and sulfate (SO_4^{2-}) were taken during spring and neap tides. Water samples for CH_4 and SO_4^{2-} were taken every 2 and 1 h, respectively, using a peristaltic pump (Solinst). Samples for dissolved CH_4 were collected with a 60-mL plastic syringe, transferred into 22-mL

glass vials, and preserved with ZnCl_2 avoiding any headspace. Samples for $\delta^{13}\text{C}-\text{CH}_4$ measurements were collected in 60-mL serum bottles and overflowed a few times before adding 100 μL of HgCl_2 solution. The bottles were immediately crimped with butyl rubber stoppers. All the samples were kept cold before analysis. Discrete samples for SO_4^{2-} were collected in 15-mL falcon tubes.

Sediment coring and porewater sampling

To identify the sources of CH_4 and potential oxidation within sediments, sediment cores and seep waters were collected. Seeping creek water ($n = 10$) flowing out from the bank of the creek and crab burrows during low tide were sampled at M1. At M2, ~ 50 cm deep bores were dug by shovel and purged 2–3 times using a peristaltic pump before collecting seeping porewaters ($n = 10$). We categorized these bore samples as seeps because bores collected water from nearby burrows. CH_4 concentration, $\delta^{13}\text{C}-\text{CH}_4$ and SO_4^{2-} were collected for seeps and preserved similar to surface waters.

In each mangrove, we collected three sediment cores from lower (closer to creek, seaward), middle and upper (landward) sections. One core was used for CH₄ concentration and isotope analyses, one core was used for porewater chemistry, and the last core for sediment density. Sediment cores (~1 m) were collected using manual hammering of a PVC push corer. For porewater CH₄ sampling, predrilled PVC cores (resolution of 5–10 cm) were used. Then, 3 mL of wet sediments were collected using a cut-off syringe. The sediment was immediately transferred to 22-mL glass vials filled with 10 mL of 1 M NaOH and saturated ZnCl₂. Vials were crimped with butyl rubber stoppers and weighed.

For porewater chemistry, sediment was collected from a predrilled PVC corer. Upon retrieval of the sediment cores, Rhizon samplers (Rhizosphere) were inserted into predrilled holes at 10-cm intervals. Porewater was extracted from the sediment cores using polyethylene syringes. The sampling depth was around 60 to 100 cm. Approximately 5–10 mL of porewater were collected at each depth and transferred to 3- and 2-mL vials for dissolved inorganic carbon (DIC) and SO₄²⁻ analysis. The samples were kept cold for further analysis. Another sediment core was sliced for dry bulk density at every 10 cm, which was determined by the weight of dry mass over the volume of sediment.

Laboratory analysis

Back in the laboratory, CH₄ concentrations were determined using headspace techniques. For surface water and seep samples, 5 mL of water samples were withdrawn using a syringe while simultaneously injecting N₂ gas into the vials to create headspace. Vials with porewater already contained a headspace and did not require any pretreatment. All vials were inverted overnight to ensure equilibrium. The headspace was analyzed by a gas chromatograph (Thermo Scientific Trace 1300) equipped with a flame ionization detector (FID). Each measurement run was calibrated with gas standards of 1.9 and 50.0 ppm of CH₄ (Air Liquide Gas AB). For seep samples, headspace was measured by another gas chromatograph (SRI 8610C) with FID, calibrated with 1, 10, 30, 509, and 2010 ppm of CH₄ (Air Liquide Belgium). The solubility coefficients of CH₄ was used to convert from partial pressure to dissolved CH₄ concentration (nM) according to Weiss (1974) and Yamamoto et al. (1976). Porewater DIC was determined by a total dissolved inorganic carbon analyzer (Apollo SciTech AS-C5) with certified reference materials (Dickson Laboratory, Scripps Institute of Oceanography). SO₄²⁻ was measured using ion chromatography.

Isotope analysis

The headspace from porewater CH₄ samples was transferred to the pre-evacuated 12-mL exetainer (Labco) vials for δ¹³C-CH₄. The headspace was then injected into a cavity ring-down spectrometer (G2201-I, Isotopic Analyzer, Picarro) with a

Small Sample Introduction Module 2 (SSIM, Picarro). Data were calibrated with two gas standards from Airgas Speciality Gases with certified δ¹³C-CH₄ values of −23.9‰ ± 0.3‰ and −69.0‰ ± 0.3‰. To ensure the headspace fell within the recommended operation range, it was diluted to below 10 ppm if necessary. The δ¹³C-CH₄ is expressed as a ratio of δ¹³C in the sample relative to the international standard (Vienna Pee Dee belemnite).

Water–air and porewater CH₄ flux calculation

The water–air CH₄ fluxes were determined using CH₄ concentrations in air and water, and gas transfer velocities:

$$F_{CH_4} = K_{600} \left(\frac{Sc}{600} \right)^{-0.5} k_0 (P_W - P_a), \quad (1)$$

where FCH₄ is the water–air CH₄ fluxes (μmol m⁻² d⁻¹), K₆₀₀ is the gas transfer velocity (cm h⁻¹) and normalized to a Schmidt number (Sc) of 600 (Wanninkhof 2014). k₀ is the solubility of CH₄ (Yamamoto et al. 1976), P_W and P_a are the partial pressure of CH₄ measured in water and atmosphere, respectively. We assumed CH₄ atmospheric pressure (P_a) as 1.9 ppm, obtained from NOAA (Lan et al. 2023).

The gas transfer velocity model (K₆₀₀) accounts for various drivers of turbulence such as wind speed, current, and depth (Supporting Information Table S2). Since water–air fluxes were greatly influenced by the gas transfer velocity model, we calculated a potential range of water–air CH₄ fluxes using six different gas transfer equations from literature (Borges et al. 2004; Ho et al. 2016; Rosentreter et al. 2017; Jeffrey et al. 2018). These models offer a potential range of CH₄ transfer velocities and enable comparisons with other studies. The average of the six models is taken as the most likely water–air CH₄ flux. Hourly wind speeds used in the parameterization of gas transfer velocities were provided by local meteorological stations at 10 m height (A619—23°13′25.8″S, 44°43′31.8″W and A806—27°36′09.6″S, 48°37′12.3″W) from the Brazilian Institute of Meteorology (INMET, 2023).

Porewater exchange rate refers to the lateral seepage of porewater to tidal creek surface waters. A radon mass balance model was used to estimate the porewater exchange rate as explained in a companion manuscript (Cabral et al. 2024 and references therein). The model accounts for all the known radon sources and sinks in and out of the creek, and assumes that any missing radon was due to porewater exchange. The porewater-derived CH₄ flux (FCH₄PW) (μmol mangrove m⁻² d⁻¹) was calculated based on the porewater exchange rate obtained from the radon mass balance model (cm d⁻¹) and the porewater CH₄ endmember (μM), then were corrected for the average water intertidal mangrove surface area (m²) (Santos et al. 2019). The area of intertidal mangroves was estimated using satellite images (Google Earth Pro 2023). Because porewater exchange in mangroves is driven by advective

seawater circulation in sediments over tidal time scales (Call et al. 2019), the porewater CH₄ endmember was defined as the CH₄ difference between average porewater concentration and the average surface water concentration at high tide (Santos et al. 2019). The porewater endmember thus represents the net CH₄ enrichment after seawater penetration into sediments.

CH₄ oxidation calculations

Isotope enrichment behaves differently under closed and open system conditions. An open system model assumes that CH₄ is produced in one reservoir (e.g., surface sediments) and oxidizes in another reservoir (e.g., surface water) (Eqs. 2, 3). We employed two models under open system assumptions at steady state (Happell et al. 1994; Tyler et al. 1997) (Eqs. 2, 3, 5, 6). A closed system model assumes that CH₄ is removed from the 1st reservoir (e.g., surface sediments) and accumulates in the 2nd reservoir (e.g., surface water) until all CH₄ is consumed (Eqs. 4, 7). This approach was also applied in recent study of oxidation in Australian mangroves (Cotovicz et al. 2024). To estimate the fraction of CH₄ (being oxidized in surface water (f_{oxW}), we used the difference in $\delta^{13}C$ -CH₄ between surface water (δ_{water}) and the two potential endmembers (δ_{PWsurf}), seeps and deep porewater (>50 cm, δ_{PWdeep}) (Eqs. 2–4; Supporting Information Table S5).

$$f_{oxW} = \frac{(\delta_{water} - \delta_{PWsurf})}{((\alpha - 1) \times 1000)}, \quad (2)$$

$$f_{oxW} = \frac{(\delta_{PWsurf} - \delta_{water})}{(\delta_{water} + 1000) \times \left(\frac{1}{\alpha} - 1\right)}, \quad (3)$$

$$\ln(1 - f_{oxW}) = [\ln(\delta_{PWsurf} + 1000) - \ln(\delta_{water} + 1000)] / [\alpha - 1]. \quad (4)$$

For oxidation in surface sediments (f_{oxS}), we calculated the $\delta^{13}C$ -CH₄ difference between surface porewater (>20 cm, δ_{PWsurf}) and deep porewater (>50 cm, δ_{PWdeep}) (Euler et al. 2023) (Eqs. 5–7; Supporting Information Table S5). Note that oxidation could only be estimated when the CH₄ endmember (deep porewater) is more depleted in ^{13}C ($\delta^{13}C$ -CH₄ more negative) than the remaining pool of CH₄. We grouped the sediment into surface (<20 cm), intermediate (20–50 cm) and deep porewater (>50 cm) according to CH₄ distribution profiles.

$$f_{oxS} = \frac{(\delta_{PWsurf} - \delta_{PWdeep})}{(\alpha - 1) \times 1000}, \quad (5)$$

$$f_{oxS} = \frac{(\delta_{PWdeep} - \delta_{PWsurf})}{(\delta_{PWsurf} + 1000) \times \left(\frac{1}{\alpha} - 1\right)}, \quad (6)$$

$$\ln(1 - f_{oxS}) = [\ln(\delta_{PWdeep} + 1000) - \ln(\delta_{PWsurf} + 1000)] / [\alpha - 1]. \quad (7)$$

The fractionation factor (α) is used to estimate the degree of isotopic enrichment. We determined α based on (1) in situ porewater temperature (Eq. 8) (Chanton and Liptay 2000) and (2) fractionation factor of 1.025, the lower limit previously applied to wetlands (Ward et al. 2020). We assume a same ^{13}C fractionation factor in the case of aerobic and anaerobic CH₄ oxidation.

$$\alpha = (-0.000433 * T) + 1.0421. \quad (8)$$

The oxidation of CH₄ ($\mu\text{mol m}^{-2} \text{d}^{-1}$) in the creek water (MOX_w , Eq. 9) and surface sediment (MOX_{sed} , Eq. 10) was estimated using the oxidation fractions (f_{oxW} , f_{oxS}) and CH₄ fluxes (FCH_4 , FCH_4PW):

$$MOX_w = f_{oxW} \times FCH_4 / (1 - f_{oxW}), \quad (9)$$

$$MOX_{sed} = f_{oxS} \times FCH_4PW / (1 - f_{oxS}). \quad (10)$$

Linear regression analysis was performed to determine the relationships between CH₄ concentration and $\delta^{13}C$ -CH₄ with environmental parameters (lm function in R). For the regression analyses of $\delta^{13}C$ -CH₄, we separate the surface water data into spring ($n = 15$ at M1 and $n = 16$ at M2) and neap ($n = 18$ at M1 and $n = 14$ at M2) at each site. p -values of < 0.05 were assumed to represent significant correlations. Statistics and graphs were done using R statistical package (R Core Team 2021).

Results

Time series observations

Both mangrove creeks exhibited temporal variations in environmental parameters. Water depth oscillated from 0.6 to 2.2 m and from 1.5 to 2.4 m in M1 and M2, respectively (Fig. 2). Salinity varied in M1 from 22 to 35, influenced by accumulated rainfall of 58 mm during the sampling period. M2 recorded lower salinity fluctuations (29–34), with the accumulated rainfall of only 6 mm during the sampling period. Water temperature was 2°C higher in M2 than M1 (Table 1). Current velocities were higher in M2 than M1, with maximum velocities ($\sim 80 \text{ cm s}^{-1}$) during spring tides. DO saturation followed tidal oscillations in M1 with undersaturation during low tide and oversaturation during high tide (Fig. 2). In contrast, M2 displayed diel cycles in DO saturation, with supersaturation during the day and undersaturation at night (Supporting Information Fig. S1). ^{222}Rn displayed tidal patterns at both sites with the highest concentration during low tide (Fig. 2).

Dissolved CH₄ in mangrove creeks

CH₄ fluctuated from 2.3 to 50 nM in M1 and 2.6 to 190 nM in M2 (Fig. 2). CH₄ concentrations at both sites followed tidal patterns, with peak concentrations observed

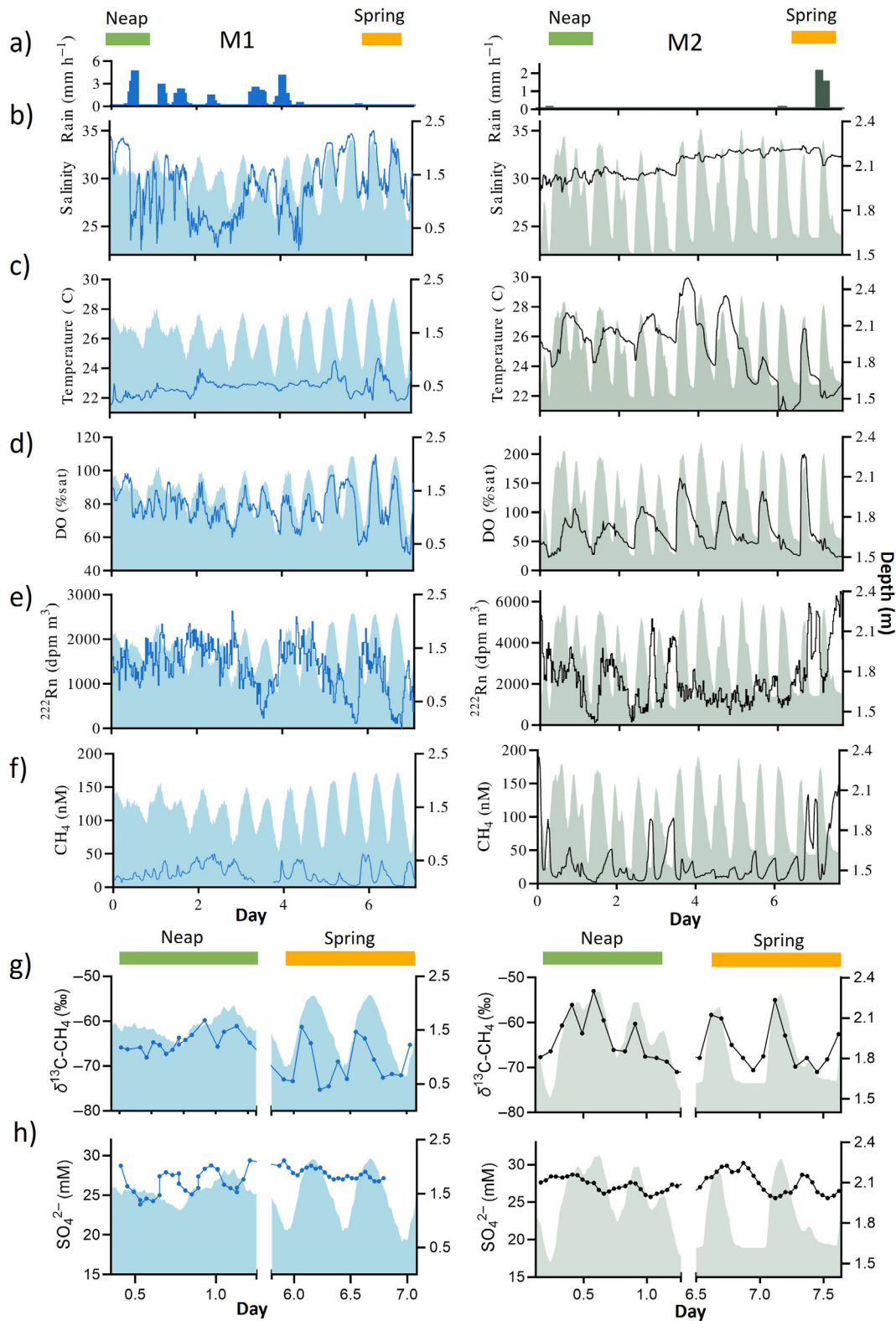


Fig. 2. Surface creek water time series observations of (a) salinity, (b) temperature, (c) dissolved oxygen saturation, (d) radon concentration, and (e) CH₄ at M1 and M2 mangrove in Brazil. The data were smoothed to 30 min. Discrete samples of δ¹³C-CH₄ (f) and sulfate (g) were collected only during spring and neap tide. The bar on top indicates neap and spring tides. The shaded area in each graph represents the water depth. Radon data originally reported in Cabral et al. (2024). All the methane data are original.

Table 1. Average \pm SD (range) of environmental parameters and water-air CH₄ fluxes in both mangrove sites. Different parameterization of gas transport models was used (Table S2). Data were smoothed to 30 minutes.

		M1	M2
Water depth	m	1.5 \pm 0.4 (0.6–2.2)	1.9 \pm 0.2 (1.5–2.4)
Tidal range	m	1.61	0.85
Water temperature	°C	22.7 \pm 0.6 (21.5–24.7)	25.2 \pm 2.1 (21.0–30.0)
Salinity		29.1 \pm 3.1 (22.4–35.0)	31.6 \pm 1.3 (28.5–33.5)
Wind speed	m s ⁻¹	1.2 \pm 0.8 (0.1–3.8)	1.8 \pm 1.2 (0.1–5.6)
Current velocity	cm s ⁻¹	30.6 \pm 14.5 (11–99)	34.0 \pm 18.5 (0.1–105.7)
DO	mg L ⁻¹	5.7 \pm 0.8 (3.5–7.9)	4.6 \pm 2.4 (1.6–14.3)
Oxygen saturation	%	78 \pm 11 (49–110)	68 \pm 36 (22–223)
CH ₄	nM	20.2 \pm 13 (2.3–50)	31.6 \pm 35 (2.6–190)
SO ₄ ²⁻ ^a	mM	27.0 \pm 2.3 (18.8–31.4)	27.4 \pm 2.2 (20.0–33.5)
$\delta^{13}\text{C-CH}_4$ ^b	‰	-66.9 \pm 4.2 (-61.3–75.3)	-64.8 \pm 5.0 (56.1–71.0)
²²² Rn	dpm m ⁻³	1354 \pm 538 (118–2626)	2195 \pm 1319 (112–6491)
Water-air CH₄ flux			
Ho et al., (2016)	$\mu\text{mol m}^{-2} \text{d}^{-1}$	17 \pm 15 (0–87)	34 \pm 39 (0.3–214)
Rosentreter et al., (2017) ^c	$\mu\text{mol m}^{-2} \text{d}^{-1}$	50 \pm 39 (0–209)	114 \pm 153 (1–939)
Rosentreter et al., (2017) ^d	$\mu\text{mol m}^{-2} \text{d}^{-1}$	57 \pm 45 (0–246)	128 \pm 176 (1–1122)
Rosentreter et al., (2017) ^e	$\mu\text{mol m}^{-2} \text{d}^{-1}$	62 \pm 47 (0–235)	125 \pm 180 (0–1942)
Borges et al., (2004)	$\mu\text{mol m}^{-2} \text{d}^{-1}$	52 \pm 41 (0–228)	99 \pm 112 (1–597)
Jeffrey et al., (2018)	$\mu\text{mol m}^{-2} \text{d}^{-1}$	68 \pm 65 (0–266)	152 \pm 204 (1–1250)
Average of 6 models	$\mu\text{mol m}^{-2} \text{d}^{-1}$	51 \pm 41	109 \pm 151

^aMeasurements conducted only during spring and neap tide.

^bMeasurements only conducted during spring and neap tide, sample size of M1 and M2 are 33 and 30, respectively.

^cModel equation includes only wind speed, current velocity, and water depth.

^dModel equation includes only wind speed, current velocity.

^eModel equation includes only current velocity.

during low tide and the lowest during high tide at both sites (Fig. 3; Supporting Information Fig. S1). Low-tide CH₄ concentrations at M2 was 3 times higher in spring than neap tide, while ²²²Rn was 1.6 times higher during spring tide (Supporting Information Table S3). M1 did not show a clear

spring-neap variation in CH₄ and ²²²Rn concentration (Fig. 3; Supporting Information Table S3).

At both sites, CH₄ concentrations were significantly and positively correlated with ²²²Rn ($R^2 = 0.44$ at M1; $R^2 = 0.69$ at M2) (Fig. 3; Supporting Information Figs. S4, S5). At M1, CH₄ showed a negative correlation with salinity ($R^2 = 0.52$) and DO saturation ($R^2 = 0.35$) (Fig. 3). In contrast, M2 displayed a negative correlation between CH₄ and water depth ($R^2 = 0.28$) (Fig. 3). While the correlations with CH₄ concentrations appear linear (Fig. 3), anticlockwise hysteresis loops occur over multiple tidal cycles indicating a delayed increase in CH₄ during low tide (Supporting Information Figs. S2, S3). Spatial variation was also observed (Table 1). Both ²²²Rn and CH₄ were 1.6 times higher in M2 than M1. Both creeks were oversaturated in CH₄ and acted as sources of CH₄ to the atmosphere. Water-air CH₄ fluxes in M1 ($51 \pm 41 \mu\text{mol m}^{-2} \text{d}^{-1}$) were half of those in M2 ($109 \pm 151 \mu\text{mol m}^{-2} \text{d}^{-1}$) (Table 1).

$\delta^{13}\text{C-CH}_4$ in water column

Creek water $\delta^{13}\text{C-CH}_4$ values in M1 and M2 ranged from -61.3‰ to -75.3‰ and -56.1‰ to -71.0‰, respectively (Table 1). $\delta^{13}\text{C-CH}_4$ values exhibited tidal trends (Fig. 2) and an inverse relationship with CH₄ concentrations in both mangrove sites (Fig. 4c). Water depth was positively correlated with $\delta^{13}\text{C-CH}_4$ at both sites (Fig. 4). Spring tides were associated with ¹³C-depleted CH₄ at M1 due to higher porewater exchange with surface creek waters (Fig. 2; Supporting Information Table S3). $\delta^{13}\text{C-CH}_4$ exhibited a significant positive correlation with O₂ saturation only during spring tides at M1 ($R^2 = 0.41$, $p = 0.01$) (Fig. 4b). During spring low tide, M1 also was more depleted in ¹³C (-70‰ \pm 2‰) than high tide, approaching the average values in seeps (-74.2‰ \pm 3.5‰) (Fig. 4).

Porewater endmember

The average CH₄ concentration and $\delta^{13}\text{C-CH}_4$ in seeps were $4.5 \pm 10.8 \mu\text{M}$ and -74.2‰ \pm 3.5‰, respectively, in M1 (Table 2). The calculated $\delta^{13}\text{C-CH}_4$ values of porewater endmember using Keeling plots (M1: -71.8‰, M2: -67.9‰) (Fig. 4c) were within 2–3‰ of measured seep values at both M1 (-74.2‰ \pm 4.5‰) and M2 (-63.5‰ \pm 4.8‰) during spring tides. The ¹³C enrichment during spring tide at both sites indicates a strong porewater signal during low tide. Surface sediments in M1 and M2 were up to 200 times more enriched in CH₄ than surface waters (Tables 1, 3).

Porewater CH₄ from sediment cores ranged from 1.4 to 403 μM and 3 to 158 μM in M1 and M2, respectively (Fig. 5). Porewater CH₄ varied between 1 and 50 μM at the first 50 cm, but increased sharply from 50 to 100 cm at M1 (Fig. 5). In contrast, M2 showed a CH₄ peak at 20–30 cm deep (Fig. 5). A positive trend was observed between sediment depth and porewater CH₄ (Supporting Information Fig. S7). Porewater DIC in M1 showed a gradual increase from 10 to 30 mM within the top 50 cm, while porewater SO₄²⁻ remained consistent throughout the sediment depth (Fig. 5). Porewater CH₄

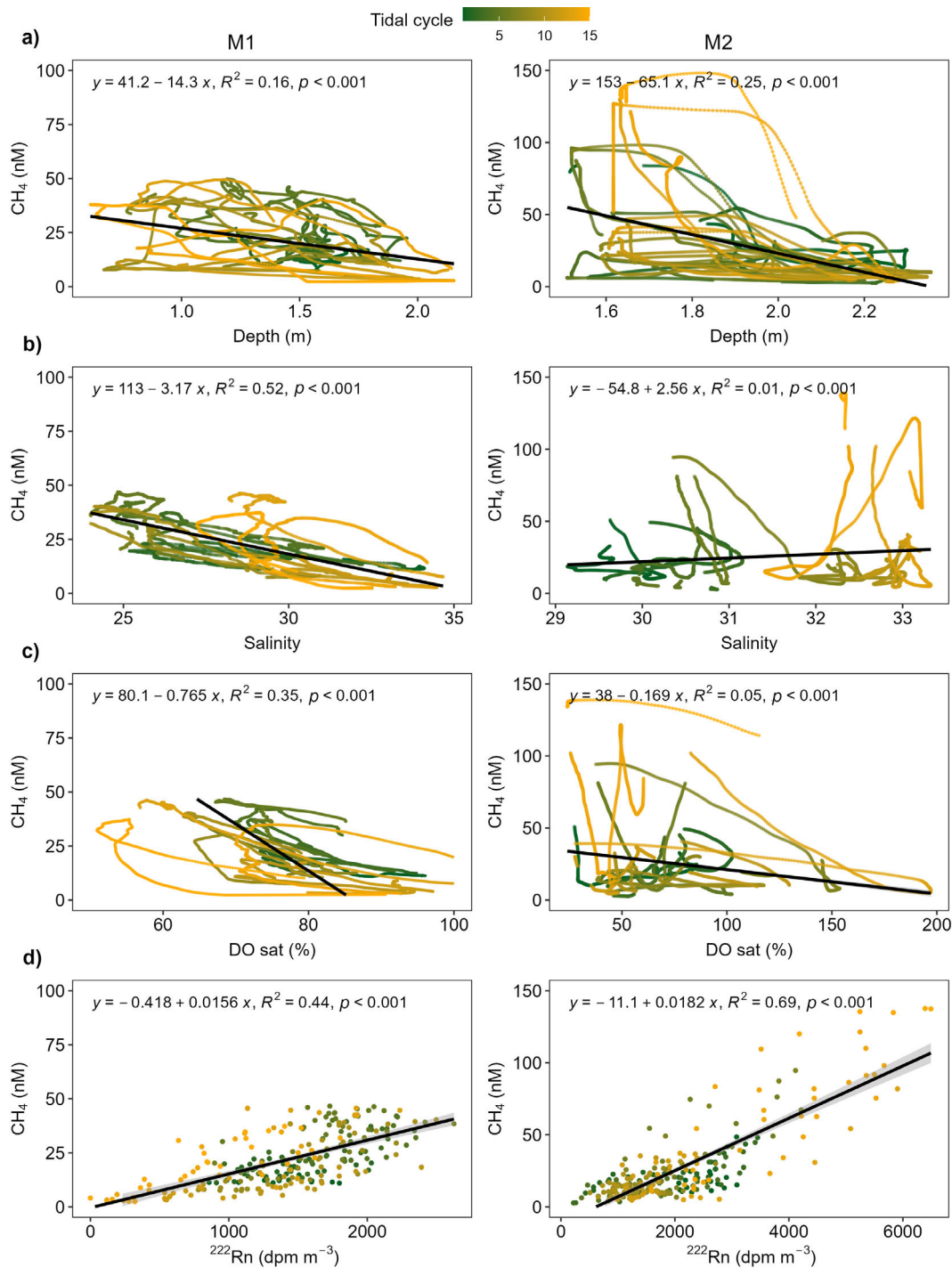


Fig. 3. Scatter plots of CH₄ with (a) water depth, (b) salinity, (c) dissolved oxygen saturation, and (d) ^{222}Rn at both sites. The color gradient indicates the tidal cycle number with neap being the first three tidal cycles (green) and spring tide being last three cycles (yellow) (see also Fig. 2). The data were smoothed to 30 min. Black straight lines and shaded areas represent linear regressions of all data and 95% confidence intervals, respectively. Spring and neap tide tidal loops are shown in Supporting Information Figs. S2 and S3.

and DIC concentrations were 8 and 4 times greater in M1 than M2, respectively.

Porewater-derived CH₄ fluxes in M1 and M2 were 476 ± 1170 and $10 \pm 11 \mu\text{mol mangrove m}^{-2} \text{d}^{-1}$, respectively

(Table 2) using radon-derived porewater-exchange rates from Cabral et al. (2024). Yet, water-air CH₄ fluxes exhibited an opposite trend compared to porewater CH₄ fluxes between the mangrove sites as M1 had a 3 times lower water-air CH₄ flux

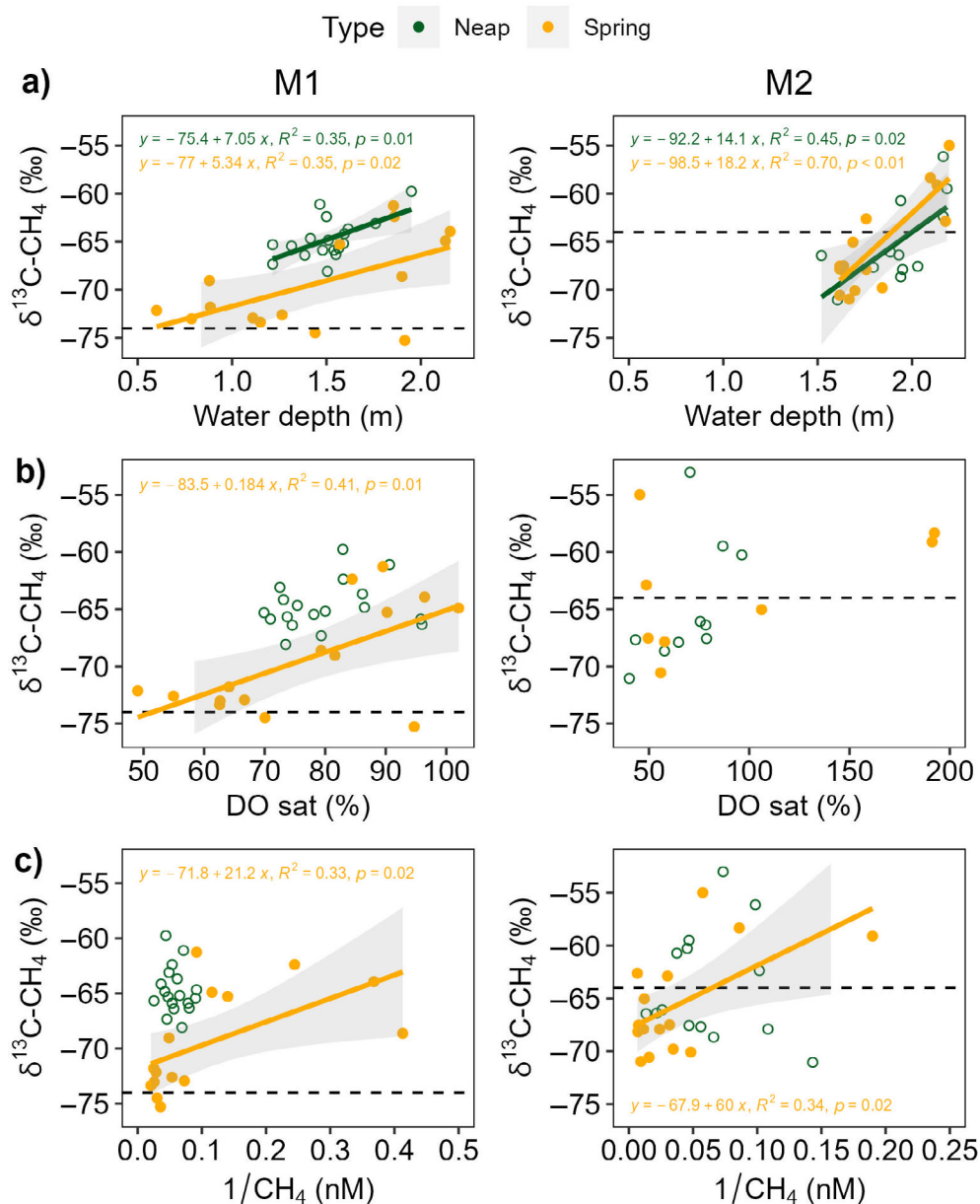


Fig. 4. Correlations between $\delta^{13}\text{C-CH}_4$ and (a) water depth, (b) dissolved oxygen saturation, (c) inverse of CH_4 concentration (keeling plot). The data were grouped by spring (solid circle) and neap tide (open circle) (Fig. 2). The horizontal dotted line represents $\delta^{13}\text{C-CH}_4$ of surface porewater endmember with -74‰ and -64‰ in M1 and M2, respectively (Table 2). Solid line indicates significant linear regression with shaded area corresponding to 95% confidence intervals. The intercept of regression line of keeling plot represents the calculated $\delta^{13}\text{C-CH}_4$ value of the CH_4 source (Pataki et al. 2003).

than M2 (Table 2). In M1, lateral porewater-derived CH_4 fluxes exceeded water-air fluxes by 9 times, while M2 showed a much lower porewater contribution, with porewater-derived CH_4 fluxes 6 times lower than water-air fluxes (Tables 2, 3). This implies that some of the porewater-derived methane is oxidized, or exported to the coastal ocean where it can escape to the atmosphere.

Methane oxidation in water and sediment

The average $\delta^{13}\text{C-CH}_4$ values in creek surface water were $\sim 10\text{‰}$ less negative than in surface porewater from M1. In contrast, $\delta^{13}\text{C-CH}_4$ in creek surface water in M2 ($-64.8\text{‰} \pm 5.0\text{‰}$) exhibited a similar signal as seeps ($-63.5\text{‰} \pm 4.8\text{‰}$) (Table 2; Fig. 6). In M1, assuming surface porewater and deep porewater as the CH_4 source, 30–58% of CH_4 from porewater

Table 2. Summary of CH₄ and environmental parameters of seeps and sediment core at both mangrove sites. Average ± SD was presented. *n* represents the number of discrete samples.

	Unit/depth	M1	M2
Seeps			
Salinity		<i>n</i> = 10 24.3 ± 2.7	<i>n</i> = 10 31.4 ± 0.7
Temperature	°C	24 ± 1	22 ± 1
pH		6.9 ± 0.6	6.1 ± 0.1
SO ₄ ²⁻	mM	23.1 ± 1.3	28 ± 0.7
CH ₄	μM	4.5 ± 10.8	0.6 ± 0.4
δ ¹³ C-CH ₄	‰	-74.2 ± 3.5	-63.5 ± 4.8 ^a
Sediment core			
Dry bulk density	g cm ⁻³	<i>n</i> = 3 0.26 ± 0.01	<i>n</i> = 3 0.5 ± 0.1
CH ₄	μM		
0–20 cm	Surface	10.1 ± 12 (<i>n</i> = 6)	54.1 ± 106.5 (<i>n</i> = 6)
20–50 cm	Intermediate	22.3 ± 15.9 (<i>n</i> = 12)	17.8 ± 11.2 (<i>n</i> = 8)
50–90 cm	Deep	123.8 ± 102.7 (<i>n</i> = 14)	31.7 ± 48.2 (<i>n</i> = 11) ^a
δ ¹³ C-CH ₄	‰		
0–20 cm	Surface	-74.3 ± 6	-56.0 ± 2.1
20–50 cm	Intermediate	-77.5 ± 5.1	-57.4 ± 6.8
50–90 cm	Deep	-83.0 ± 3.7	-69.4 ± 6.3
Porewater exchange rate ^c	cm d ⁻¹	10.7 ± 3.9	2.3 ± 1.4
Porewater-derived CH ₄ flux ^d	μmol mangrove area m ² d ⁻¹	476 ± 1174	10 ± 11

^aOnly 2 sediment cores were used for analysis.

^bOnly deep sediments were used to calculate the fraction and Eq. 8 was used.

^cPorewater flux was derived from ²²²Rn mass balance from (Cabral et al. 2024).

^dPorewater-derived CH₄ fluxes was estimated by multiplying the radon-derived porewater exchange by porewater endmember. Porewater endmember is the average CH₄ in porewater minus the average CH₄ in surface water. The fluxes were corrected with the entire intertidal area of mangrove creek, area was estimated as 260,112 and 146,065 m² (Table S4).

was oxidized in surface water (Table 3). In M1, the fraction of CH₄ oxidation had a positive correlation with water depth and DO (Figure 7). For M2, 63% of surface water samples were more depleted in ¹³C (-59.8‰ to -72.9‰) than the endmember value of surface sediment (-63.5‰), preventing calculations of the oxidation percentage for those samples (Fig. 6; Table 3). This also suggested that we may have not

Table 3. Estimated CH₄ oxidation percentages and CH₄ oxidation fluxes in mangrove surface water and sediments using open system and fractionation factors from literature (Chanton and Liptay 2000; Ward et al. 2020). The averages and standard deviations (±SD) were calculated using two fractionation factors (1.025, 1.032) (Eq. 8) and two different open steady-state models (Eq. 2,3,5,6). CH₄ oxidation in surface water was estimated using two different endmember (seep and deep porewater). *n* represents the number of discrete samples collected. *ox* represents the number samples oxidized. Estimated oxidation using closed system assumptions are provided in Table S6.

	M1	M2
Percentage of CH ₄ oxidized in surface water (%) ^a	<i>n</i> = 33	<i>n</i> = 30
-Surface porewater as endmember	30 ± 14 (<i>ox</i> = 31)	17 ± 12 (<i>ox</i> = 11)
-Deep porewater as endmember	58 ± 15 (<i>ox</i> = 33)	18 ± 17 (<i>ox</i> = 24)
CH ₄ oxidation fluxes in surface water (μmol m ⁻² d ⁻¹) ^b	<i>n</i> = 6	<i>n</i> = 4
-Surface porewater as endmember	10 ± 8	3 ± 2
-Deep porewater as endmember	25 ± 25	5 ± 5
Percentage of CH ₄ oxidized in sediment (%) ^c	61 ± 16	45 ± 10
CH ₄ oxidation fluxes in sediment (μmol m ⁻² d ⁻¹) ^d	290 ± 77	9 ± 2

^aEq 2,3.

^bEq 9.

^cEq 5,6, M1 and M2 was based on 3 and 2 sediment cores, respectively.

^dEq 10.

accounted for all potential CH₄ sources in M2 such as terrestrial groundwater seepage. For surface water with δ¹³C-CH₄ higher than -63.5‰, 17% of CH₄ from porewater was being oxidized in surface water (Table 3). The estimated CH₄ oxidation rates in surface water were 10 ± 8 and 3 ± 2 μmol m⁻² d⁻¹ at M1 and M2, respectively (Table 3). Surface water CH₄ oxidation reduced 17 - 58% of the water-air fluxes in M1 and M2, respectively (Table 3).

CH₄ was more ¹³C-enriched (less negative) in shallow porewater compared to deep porewater at both mangroves (Fig. 6; Table 3). In M1, δ¹³C-CH₄ in the surface porewater was 10‰ higher than in deep porewater. 61% and 45% of CH₄ oxidation was estimated between surface and deep porewater in M1 and M2, respectively (Table 3). In M2, higher oxidation occurred in shallow porewaters (45%) than surface waters (17–18%) (Table 3). The estimated CH₄ oxidation rates in sediments were 290 ± 77 and 9 ± 2 μmol m⁻² d⁻¹ at M1 and M2, respectively (Table 3).

Discussion

Porewater as a source of CH₄

Tidally driven porewater exchange controlled creek water CH₄ dynamics on both semi-diurnal (high-low tide) and

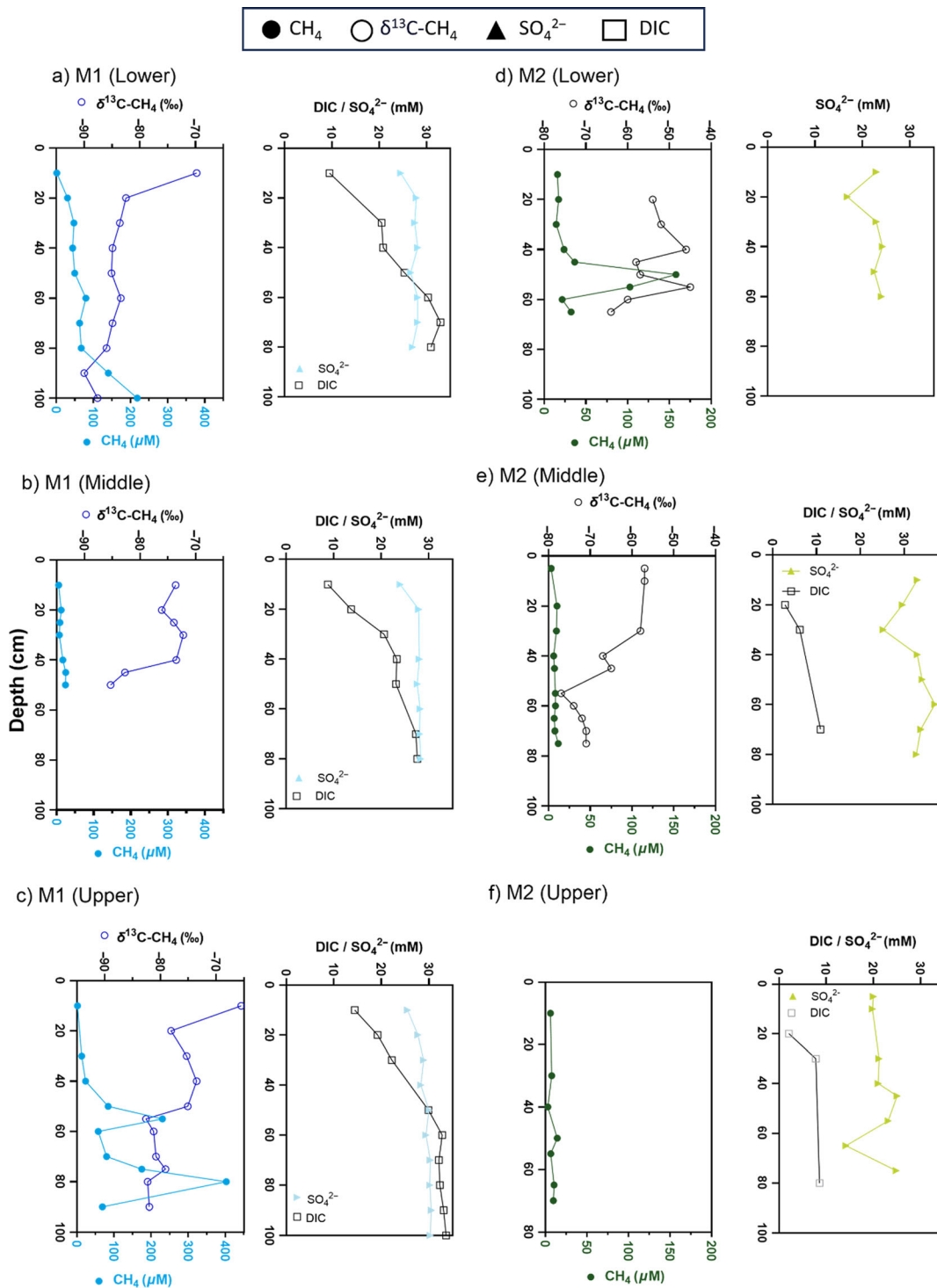


Fig. 5. Porewater profiles of CH₄, δ¹³C-CH₄, and SO₄²⁻, DIC at lower (interior), middle and upper fringe of M1 (a-c) and M2 (d-f) site. There are no δ¹³C-CH₄ and DIC data for M2 upper site and M2 lower site, respectively. The measurement accuracy for DIC and CH₄ is better than 0.1% and 3%. We did not have replicates for each site due to small porewater volumes.

biweekly (spring-neap) timescales. 5Radon, a natural porewater tracer showed a positive correlation with CH₄ concentration at both sites (Fig. 3). The more ¹³C-depleted CH₄ at

low tide matched δ¹³C-CH₄ values of seep waters (Fig. 4), further suggesting that CH₄-enriched porewater seeps out of sediments. Similar observations of ¹³C-depleted DIC during low

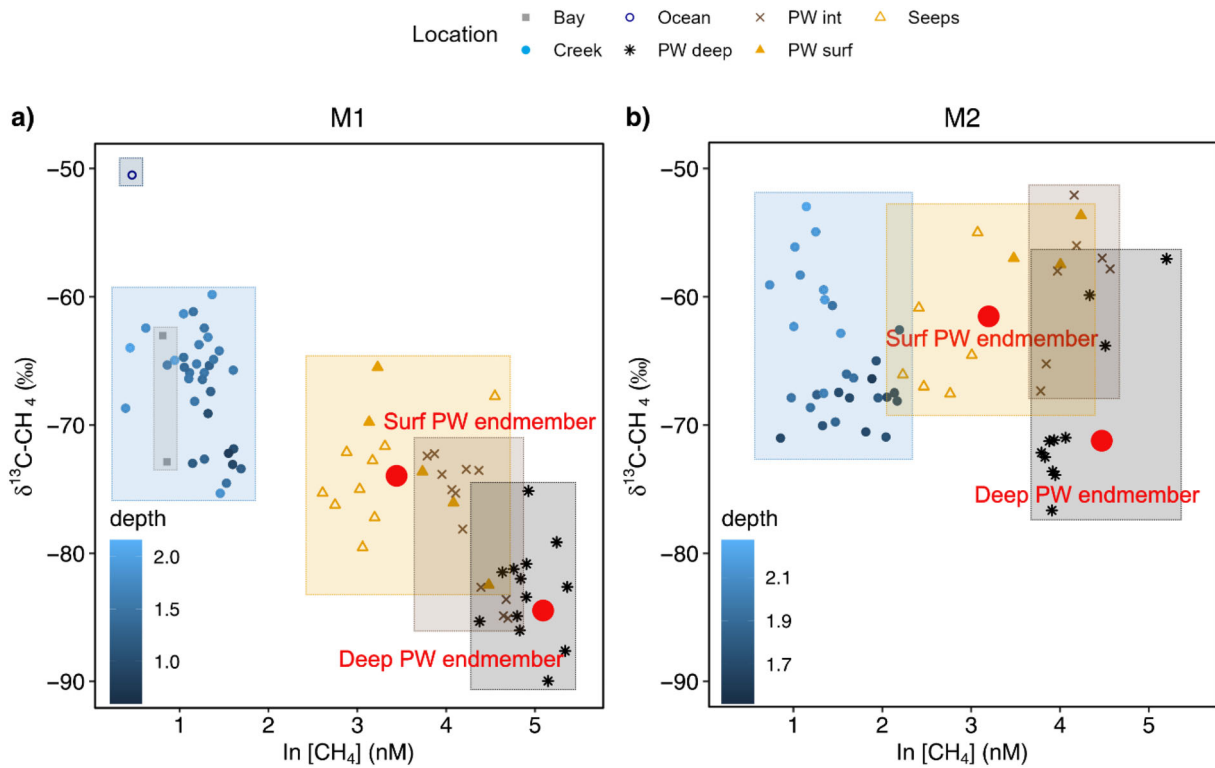


Fig. 6. Relationship between $\delta^{13}\text{C-CH}_4$ of different endmembers and the natural log-transformed CH_4 concentration in (a) M1 and (b) M2. Samples are defined as ocean, bay, creek surface water (creek), porewater surface (PW surf), porewater intermediate (PW int), porewater deep (PW deep), and seep. The shaded area indicates the ranges of $\delta^{13}\text{C-CH}_4$ and CH_4 concentration in each endmember. The blue color gradient represents water depth of surface waters. The red dot denotes the average surface and deep porewater endmember used for the oxidation calculation as presented in Supporting Information Table S5.

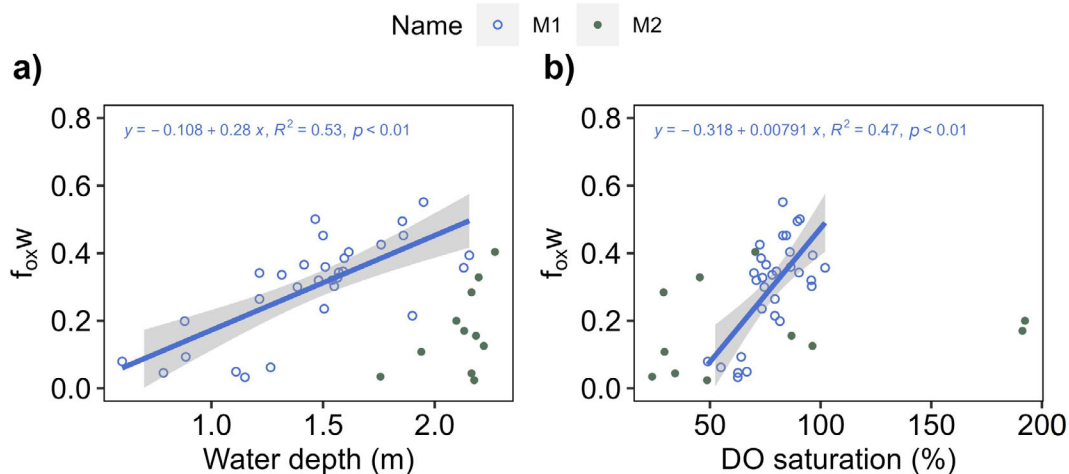


Fig. 7. Fraction of CH_4 oxidized in the surface water (f_{ox}) against (a) water depth and (b) dissolved oxygen saturation in both sites. Data points represent the average oxidation calculated from open systems using surface porewater as endmember shown in Table 3. Significant linear regressions ($p < 0.05$) are indicated by solid lines. The shaded areas indicate 95% confidence interval of the regression lines. Annotations on the graph denote the linear regression equation and fit of the model (R^2).

tide in a Tanzanian mangrove, support a porewater source to mangrove creek water (Bouillon et al. 2007). Hence, stable isotopes and ^{222}Rn corroborate earlier studies (Bouillon

et al. 2007; Call et al. 2019; Santos et al. 2019; Cotovicz et al. 2024) identifying porewater exchange as the key source of CH_4 to mangrove waters. ^{222}Rn and CH_4 concentration in

low tide increased 1.6 and 3 times from neap to spring tide at M2, respectively (Fig. 3; Supporting Information Table S3), suggesting that spring tides inundate larger areas of mangrove and facilitate the flushing of CH₄-enriched porewater into the creek due to a greater hydraulic gradient between mangrove porewater and creek (Call et al. 2019). High tidal variation of CH₄ substantiates the important role of porewater in mangroves.

Our estimated porewater fluxes were derived from a radon mass balance (Cabral et al. 2024) where all the missing radon flux was attributed to porewater exchange. The radon mass balance cannot resolve the contribution of fresh groundwater vs. porewater exchange and has uncertainties of 36–60%. Fresh groundwater could be a source of radon (Tamborski et al. 2021). However, salinity had an insignificant ($r^2 < 0.01$ at M2) or very weak correlation ($r^2 = 0.23$ at M1) with radon (Supporting Information Fig. S8). This implies that direct rainfall rather than fresh terrestrial groundwater drove the low salinity at M1 (Supporting Information Fig. S8). Differentiating porewater and groundwater fluxes would require the use of additional tracers such as radium isotopes or modeling (Guimond and Tamborski 2021; Xin et al. 2022).

Methane accumulates in porewater around the organic-rich mangrove rhizosphere (Euler et al. 2023). The highest CH₄ concentrations were found in the deeper sediment (> 60 cm) (Fig. 6). The $\delta^{13}\text{C-CH}_4$ values of the deeper sediments ($-83.0\text{‰} \pm 3.7\text{‰}$ at M1 and $-69.4\text{‰} \pm 6.3\text{‰}$ at M2) suggests the contributions from both hydrogenotrophic and acetolactic methanogenesis pathways. This coincides with the highest methanogen abundance observed in deeper sediments (~ 60 cm) of Australian mangroves (Euler et al. 2023). The anoxic and low redox potential conditions provide a suitable environment for methanogenesis. Our findings extend the depth range of the reported CH₄ accumulation in mangroves (Biswas et al. 2007; Das et al. 2018; Sánchez-Carrillo et al. 2021) and suggest that methanogenesis occurs deeper than 60 cm.

CH₄ oxidation

The surface waters were more enriched in ¹³C ($\delta^{13}\text{C-CH}_4$ becomes less negative) compared to sediments suggesting CH₄ oxidation along the porewater pathway from sediment to surface water (Fig. 6). We estimated 17–58% of CH₄ delivered from tidal pumping of mangrove was oxidized in the water column and the remaining was emitted to the atmosphere (Table 1). Overall, our estimated surface water CH₄ oxidation percentages and CH₄ oxidation rates (10 ± 8 and $3 \pm 2 \mu\text{mol m}^{-2} \text{d}^{-1}$ in M1 and M2, respectively) were comparable to oxidation percentages (10–35%) and rates (20.9 – $15.3 \mu\text{mol m}^{-2} \text{d}^{-1}$) in seawater-dominated Australian mangroves using a similar isotopic approach (Cotovicz et al. 2024).

CH₄ oxidation occurred primarily in sediments rather than in creek waters. Around half of the CH₄ (61% at M1 and 45% at M2) was consumed between deep and surface sediments

indicating that oxidation reduces CH₄-enriched porewater before it reaches surface waters. Anaerobic oxidation of methane (AOM) can oxidize part of the CH₄ in marine sediments (Iversen and Jørgensen 1985; Jørgensen et al. 2001). The enriched ¹³C on the top sediment layer of M1 could be an indicator of AOM. Since sulfate concentrations are not limiting in mangroves, AOM coupled with sulfate reduction may play a role in CH₄ oxidation and reduce CH₄ emissions to the atmosphere. Quantifying the contribution of AOM requires direct measurements that are not available.

Limited measurements are available on CH₄ oxidation in mangroves and other blue carbon ecosystems, while freshwater ecosystems have been studied more extensively (Segarra et al. 2015; Schenk et al. 2021). Our results align with the $\delta^{13}\text{C-CH}_4$ trend in sediment profiles observed in Australian mangroves (Euler et al. 2023). Their study estimated that 19–59% of CH₄ was oxidized between deep and surface sediments (Euler et al. 2023). In another Australian mangrove, surface sediments were 27‰ more enriched in ¹³C relative to surface waters, suggesting oxidation in surface sediments (Cotovicz et al. 2024). Higher CH₄ oxidation (60%) in sediment was estimated using incubation experiments in polluted Sundarbans mangroves (Das et al. 2018).

Our mangroves exhibited a lower fraction of oxidation compared to a tropical floodplain lake (Barbosa et al. 2018) and rivers (Sawakuchi et al. 2016) in Amazon, where CH₄ oxidation reached up to 100%. Our findings align with a freshwater wetland where 26% of CH₄ was oxidized from sediments to surface water under diffusive conditions and no crab burrow networks (Ward et al. 2020). Yet, highly variable oxidation rates were reported in freshwater wetlands (Guerin and Abril 2007; Sawakuchi et al. 2016; Barbosa et al. 2018; Schenk et al. 2021). Overall, oxidation in mangroves is comparable to near-shore shelf waters (50% of CH₄ oxidation) (Mao et al. 2022), but lower than often observed in freshwater wetlands.

Water levels influence methane oxidation in mangroves. During high-tide, oxygen-rich seawater infiltrates the creek bank and favors CH₄ oxidation, resulting in ¹³C enriched CH₄ (Figs. 4, 7). At low tide, the ¹³C-depleted CH₄ in creek waters overlapped with the $\delta^{13}\text{C-CH}_4$ of surface sediment endmember, indicating that porewater CH₄ is directly released to the creek water without oxidation (Fig. 4). Larger tidal ranges, deeper waters, and high porewater exchange enhance CH₄ oxidation in Australian mangroves (Cotovicz et al. 2024). Moreover, elevated CH₄ oxidation was observed during high-water conditions in Amazonian rivers, suggesting that depth increases residence time of CH₄ and favors oxidation (Sawakuchi et al. 2016).

Oxygen availability may control CH₄ oxidation in both mangrove creeks. Dissolved oxygen positively correlated with the CH₄ oxidation percentage (Fig. 7) and negatively correlated with CH₄ concentration (Fig. 3) at M1. We hypothesize that aerobic oxidation occurs in creek waters. In surface

sediments, bioturbation facilitates CH₄ oxidation, explaining more positive δ¹³C-CH₄ values in surface porewater than in deep sediments (Euler et al. 2023). Roots and crab burrows enhance O₂ and nutrient exchange in surface mangrove sediments (Glud et al. 2016; Xiao et al. 2020; Kristensen et al. 2022).

Implications: CH₄ Oxidation attenuates CH₄ emissions

The CH₄ oxidation in surface waters accounted for 20% and 3% of the water–air fluxes at M1 and M2, respectively. In a mangrove-dominated estuary in India, CH₄ oxidation estimated from incubations was 14 times higher than water–air fluxes, suggesting oxidation was the main sink of CH₄ (Dutta et al. 2015). In Amazonian lakes, CH₄ oxidation removed 58–82% of the total CH₄ input to the water column (Sawakuchi et al. 2016). CH₄ emissions to oxidation ratio ranged from 0.4 to 5.1 in rivers and estuaries (Lilley et al. 1996; Abril and Iversen 2002). High oxidation lowers potential CH₄ emissions in areas rich in clay such as estuarine turbidity maximum, muddy sediments (Guerin and Abril 2007; Sawakuchi et al. 2016), and turbid near-shore waters (Mao et al. 2022). Wind speed could also influence both oxidation and emissions with higher wind enhancing water–air fluxes while inhibiting oxidation (Abril and Iversen 2002). Thus, effective CH₄ oxidation lowers the potential emissions of CH₄ to the atmosphere by consuming some CH₄.

Our estimated water–air CH₄ fluxes from creek water in two Brazilian mangroves (51 ± 41 and $109 \pm 151 \mu\text{mol m}^{-2} \text{d}^{-1}$) were within the range observed during 24-h observations in mangrove creeks from Tanzania, India, and Australia (Biswas et al. 2007; Bouillon et al. 2007; Santos et al. 2019; Rosentreter et al. 2023; Cotovicz et al. 2024). Large but highly variable porewater fluxes (476 ± 1170 and $10 \pm 11 \mu\text{mol mangrove m}^{-2} \text{d}^{-1}$ at M1 and M2) were the major CH₄ source. Porewater CH₄ fluxes at M1 were 9 times higher than water–air fluxes, highlighting that CH₄ can escape the mangrove and reach the coastal ocean. Sediment–air CH₄ fluxes measured at a 1 km away from M1 ranged from 24 to 240 $\mu\text{mol m}^{-2} \text{d}^{-1}$ (Barroso et al. 2022), which is around 0.5–2 times higher than the water–air fluxes measured in our study but comparable to our porewater CH₄ fluxes. The spatial variability across both water–air and porewater CH₄ fluxes underscores the importance of quantifying these distinct pathways.

To further assess the climate impact of CH₄ emissions, we converted CH₄ emissions to CO₂-equivalent emissions using sustained global warming potentials (SGWP) on 20- and 100-yr time horizons (Neubauer and Megonigal 2015) (Supporting Information Table S7). Our mangroves contributed 29–61 and 13–29 g CO₂ eq m⁻² yr⁻¹ on 20- and 100-yr time horizons, respectively (Supporting Information Table S7). Previous studies relied mostly on 1-d of continuous measurements (Bouillon et al. 2008; Linto et al. 2014; Rosentreter et al. 2018) or discrete chamber observations to capture the

dominant tidal drivers of water–air CH₄ fluxes (Kristensen et al. 2008; Jacotot et al. 2018). When CH₄ water–air fluxes from those studies are upscaled to an annual cycle, they led to an interpretation that CH₄ water–air fluxes can considerably offset carbon burial in sediments over time scales of decades (Rosentreter et al. 2018). Scaling up CH₄ fluxes from a few days of observations to annual emissions creates obvious uncertainties even if the dominant tidal time scale of variability is captured. Hence, long-term observations are needed to build confidence in mangrove methane budgets and refine interpretations on how methane may offset long-term carbon burial.

We assess whether CH₄ emissions impact mangrove's behavior as a sink or source of carbon by comparing creek water CH₄ emissions in CO₂-equivalent with regional average soil carbon sequestration rates in Brazil (Hatje et al. 2023). The CO₂-equivalent water–air CH₄ fluxes from these two mangroves offset only $1.7\% \pm 1\%$ (0.7–3.1%) of the average carbon burial rate in Brazil ($540 \text{ g C}_{\text{org}} \text{ m}^{-2} \text{ yr}^{-1}$) (Hatje et al. 2023) (Supporting Information Table S7). The calculated offset rate was much lower than previous estimates (1–66%) relying on data from freshwater-dominated mangroves (Rosentreter et al. 2018) and closer to a 7% offset estimated from seawater-dominated mangroves (Cotovicz et al. 2024) similar to our systems. These low offsets can be explained by the lower water–air fluxes in high-salinity tidal creeks than in freshwater-dominated mangroves receiving upstream freshwater and CH₄ inputs (Cotovicz et al. 2024). Our low CH₄ offset has also been observed in seawater-dominated carbon rich ecosystems such as saltmarshes and seagrass meadows (Al-Haj et al. 2022; Yau et al. 2022, 2023). The large variability of CH₄ offsets to carbon sequestration in blue carbon ecosystems illustrates the need for additional observations to resolve the contribution of CH₄ to mangrove carbon budgets in a wide range of mangrove systems.

Our estimates of CH₄ emissions from the water–air interface do not represent a full CH₄ budget. Sediment–air fluxes, outwelling, bioturbation, and plant-mediated transport are other pathways contributing CH₄ in mangroves. Seawater-dominated mangroves release CH₄ both from the water column (~60%) and emerged sediments (~40%) (Cotovicz et al. 2024). Although roots and crab burrows accelerate sediment–water–atmosphere exchange (Kristensen et al. 2022), sediment–air CH₄ fluxes are more important in freshwater-influenced mangroves (Cotovicz et al. 2024). Living tree stems also act as CH₄ conduits, releasing $37.5 \pm 5.8 \mu\text{mol m}^{-2} \text{d}^{-1}$ of CH₄ in an Australian mangrove (Jeffrey et al. 2019). Incorporating different pathways such as emerged soils, aerial roots, crab burrows, plant-mediated emissions, and outwelling would provide a more comprehensive picture of CH₄ emissions and their impact on mangrove carbon sequestration.

Conclusions

High-resolution time series observations revealed diel and tidal fluctuations in CH₄ within mangrove creek waters driven

by porewater exchange, mixing and oxidation. Deep sediments near the rhizome layer exhibited high porewater CH₄ concentrations with a more ¹³C-depleted than surface sediments. Despite high CH₄ inputs from porewater, ¹³C enrichment from sediment to water revealed that oxidation attenuated CH₄ emissions. We estimated that 17–58% of porewater CH₄ oxidized in surface water, and up to 61% of CH₄ was oxidized between surface and deep sediments. Water depth and dissolved oxygen availability were the key drivers of CH₄ oxidation. Our data suggest the importance of CH₄ oxidation in minimizing CH₄ emissions from mangroves, as also observed in several freshwater wetlands. Overall, water–air CH₄ fluxes (51–109 μmol m⁻² d⁻¹) and porewater CH₄ fluxes (10–465 μmol m⁻² d⁻¹) were a small offset to local soil carbon sequestration. Other CH₄ pathways such as emerged intertidal sediments, aerial roots, and crab burrows could enhance CH₄ emissions in mangroves. Nevertheless, the overall impact of water–air CH₄ emissions remains minor relative to mangrove’s substantial carbon sequestration capacity.

Data availability statement

The data and code used can be found in a public repository: <https://doi.org/10.5281/zenodo.11403078>.

References

- Abril, G., and N. Iversen. 2002. Methane dynamics in a shallow non-tidal estuary (Randers Fjord, Denmark). *Mar. Ecol. Prog. Ser.* **230**: 171–181. doi:10.3354/meps230171
- Abril, G., and others. 2013. Export of ¹³C-depleted dissolved inorganic carbon from a tidal forest bordering the Amazon estuary. *Estuar. Coast. Shelf Sci.* **129**: 23–27. doi:10.1016/j.ecss.2013.06.020
- Al-Haj, A. N., and R. W. Fulweiler. 2020. A synthesis of methane emissions from shallow vegetated coastal ecosystems. *Glob. Chang. Biol.* **26**: 2988–3005. doi:10.1111/gcb.15046
- Al-Haj, A. N., T. Chidsey, and R. W. Fulweiler. 2022. Two temperate seagrass meadows are negligible sources of methane and nitrous oxide. *Limnol. Oceanogr.* **67**: lno.12250. doi:10.1002/lno.12250
- Barbosa, P. M., V. F. Farjalla, J. M. Melack, J. H. F. Amaral, J. S. Da Silva, and B. R. Forsberg. 2018. High rates of methane oxidation in an Amazon floodplain lake. *Biogeochemistry* **137**: 351–365. doi:10.1007/s10533-018-0425-2
- Barnes, J., and others. 2006. Tidal dynamics and rainfall control N₂O and CH₄ emissions from a pristine mangrove creek. *Geophys. Res. Lett.* **33**: L15405. doi:10.1029/2006GL026829
- Barroso, G. C., and others. 2022. Linking eutrophication to carbon dioxide and methane emissions from exposed mangrove soils along an urban gradient. *Sci. Total Environ.* **850**: 157988. doi:10.1016/j.scitotenv.2022.157988
- Bastviken, D., J. J. Cole, M. L. Pace, and M. C. Van De Bogert. 2008. Fates of methane from different lake habitats: Connecting whole-lake budgets and CH₄ emissions. *J. Geophys. Res.* **113**: 2007JG000608. doi:10.1029/2007JG000608
- Belliard, J.-P., and others. 2022. Carbon dynamics and CO₂ and CH₄ exchange in the mangrove dominated Guayas river delta, Ecuador. *Estuar. Coast. Shelf Sci.* **267**: 107766. doi:10.1016/j.ecss.2022.107766
- Biswas, H., S. K. Mukhopadhyay, S. Sen, and T. K. Jana. 2007. Spatial and temporal patterns of methane dynamics in the tropical mangrove dominated estuary, NE coast of Bay of Bengal, India. *J. Mar. Syst.* **68**: 55–64. doi:10.1016/j.jmarsys.2006.11.001
- Borges, A. V., J.-P. Vanderborght, L.-S. Schiettecatte, F. Gazeau, S. Ferrón-Smith, B. Delille, and M. Frankignoulle. 2004. Variability of the gas transfer velocity of CO₂ in a macrotidal estuary (the Scheldt). *Estuaries* **27**: 593–603. doi:10.1007/BF02907647
- Bouillon, S., J. J. Middelburg, F. Dehairs, A. V. Borges, G. Abril, M. R. Flindt, S. Ulomi, and E. Kristensen. 2007. Importance of intertidal sediment processes and porewater exchange on the water column biogeochemistry in a pristine mangrove creek (Ras Dege, Tanzania). *Biogeosciences* **4**: 311–322.
- Bouillon, S., and others. 2008. Mangrove production and carbon sinks: A revision of global budget estimates. *Global Biogeochem. Cycles* **22**: GB2013. doi:10.1029/2007GB003052
- Brandini, F., L. S. Michelazzo, G. R. Freitas, G. Campos, M. Chuqui, and L. Jovane. 2019. Carbon flow for plankton metabolism of Saco do Mamanguá Ria, Bay of Ilha Grande, a subtropical coastal environment in the South Brazil bight. *Front. Mar. Sci.* **6**: 584. doi:10.3389/fmars.2019.00584
- Cabral, A., C. H. C. Bonetti, L. H. P. Garbosa, J. Pereira-Filho, K. Besen, and A. L. Fonseca. 2020. Water masses seasonality and meteorological patterns drive the biogeochemical processes of a subtropical and urbanized watershed-bay-shelf continuum. *Sci. Total Environ.* **749**: 141553. doi:10.1016/j.scitotenv.2020.141553
- Cabral, A., and others. 2024. Tidally driven porewater exchange and diel cycles control CO₂ fluxes in mangroves on local and global scales. *Geochim. Cosmochim. Acta* **374**: 121–135. doi:10.1016/j.gca.2024.04.020
- Call, M., I. R. Santos, T. Dittmar, C. E. de Rezende, N. E. Asp, and D. T. Maher. 2019. High pore-water derived CO₂ and CH₄ emissions from a macro-tidal mangrove creek in the Amazon region. *Geochim. Cosmochim. Acta* **247**: 106–120. doi:10.1016/j.gca.2018.12.029
- Canfield, D. E., E. Kristensen, and B. Thamdrup. 2005. The methane cycle, p. 383–418. *In* *Advances in marine biology*. Elsevier.
- Castellón, S. E. M., J. H. Cattanio, J. F. Berrêdo, M. Rollnic, M. D. L. Ruivo, and C. Noriega. 2022. Greenhouse gas fluxes in mangrove forest soil in an Amazon estuary. *Biogeosciences* **19**: 5483–5497. doi:10.5194/bg-19-5483-2022
- Chanton, J., and K. Liptay. 2000. Seasonal variation in methane oxidation in a landfill cover soil as determined by an

- situ stable isotope technique. *Global Biogeochem. Cycles* **14**: 51–60. doi:10.1029/1999GB900087
- Chen, G. C., and others. 2014. Rich soil carbon and nitrogen but low atmospheric greenhouse gas fluxes from North Sulawesi mangrove swamps in Indonesia. *Sci. Total Environ.* **487**: 91–96. doi:10.1016/j.scitotenv.2014.03.140
- Chynel, M., and others. 2022. Contrasting organic matter composition in pristine and eutrophicated mangroves revealed by fatty acids and stable isotopes (Rio de Janeiro, Brazil). *Estuar. Coast. Shelf Sci.* **277**: 108061. doi:10.1016/j.ecss.2022.108061
- Cotovicz, L. C., and others. 2024. Methane oxidation minimizes emissions and offsets to carbon burial in mangroves. *Nat. Clim. Chang.* **14**: 275–281. doi:10.1038/s41558-024-01927-1
- Das, S., D. Ganguly, S. Chakraborty, A. Mukherjee, and T. Kumar De. 2018. Methane flux dynamics in relation to methanogenic and methanotrophic populations in the soil of Indian Sundarban mangroves. *Mar. Ecol.* **39**: e12493. doi:10.1111/maec.12493
- Delwiche, K. B., and others. 2021. FLUXNET-CH4: A global, multi-ecosystem dataset and analysis of methane seasonality from freshwater wetlands. *Earth Syst. Sci. Data* **13**: 3607–3689. doi:10.5194/essd-13-3607-2021
- Dutta, M. K., R. Mukherjee, T. K. Jana, and S. K. Mukhopadhyay. 2015. Biogeochemical dynamics of exogenous methane in an estuary associated to a mangrove biosphere; the Sundarbans, NE coast of India. *Mar. Chem.* **170**: 1–10. doi:10.1016/j.marchem.2014.12.006
- Euler, S., L. C. Jeffrey, D. T. Maher, S. G. Johnston, R. Sugimoto, and D. R. Tait. 2023. Methanogens limited to lower rhizosphere and to an atypical salt marsh niche along a pristine intertidal mangrove continuum. *Limnol. Oceanogr.* **68**: 2167–2182. doi:10.1002/lno.12414
- Gleeson, J., I. R. Santos, D. T. Maher, and L. Golsby-Smith. 2013. Groundwater–surface water exchange in a mangrove tidal creek: Evidence from natural geochemical tracers and implications for nutrient budgets. *Mar. Chem.* **156**: 27–37. doi:10.1016/j.marchem.2013.02.001
- Glud, R. N., P. Berg, H. Stahl, A. Hume, M. Larsen, B. D. Eyre, and P. L. M. Cook. 2016. Benthic carbon mineralization and nutrient turnover in a Scottish Sea loch: An integrative in situ study. *Aquat. Geochem.* **22**: 443–467. doi:10.1007/s10498-016-9300-8
- Google Earth Pro. 2023. [Map of Brazil]. Retrieved September 2023, from <https://earth.google.com/>
- Guerin, F., and G. Abril. 2007. Significance of pelagic aerobic methane oxidation in the methane and carbon budget of a tropical reservoir. *J. Geophys. Res.* **112**: G03006. doi:10.1029/2006JG000393
- Guimond, J., and J. Tamborski. 2021. Salt marsh hydrogeology: A review. *Water* **13**: 543. doi:10.3390/w13040543
- Happell, J. D., J. Chanton, and W. S. Showers. 1994. The influence of methane oxidation on the stable isotopic composition of methane emitted from Florida swamp forests. *Geochim. Cosmochim. Acta* **58**: 4377–4388.
- Hatje, V., and others. 2023. Vegetated coastal ecosystems in the Southwestern Atlantic Ocean are an unexploited opportunity for climate change mitigation. *Nat. Commun. Earth Environ.* **4**: 160. doi:10.1038/s43247-023-00828-z
- Ho, D. T., N. Coffineau, B. Hickman, N. Chow, T. Koffman, and P. Schlosser. 2016. Influence of current velocity and wind speed on air–water gas exchange in a mangrove estuary. *Geophys. Res. Lett.* **43**: 3813–3821. doi:10.1002/2016GL068727
- Hoehler, T. M., M. J. Alperin, D. B. Albert, and C. S. Martens. 1994. Field and laboratory studies of methane oxidation in an anoxic marine sediment: Evidence for a methanogen-sulfate reducer consortium. *Global Biogeochem. Cycles* **8**: 451–463. doi:10.1029/94GB01800
- Holmes, M. E., J. P. Chanton, M. M. Tfaily, and A. Ogram. 2015. CO₂ and CH₄ isotope compositions and production pathways in a tropical peatland: δ¹³C in CH₄ and CO₂ in tropical peat. *Global Biogeochem. Cycles* **29**: 1–18. doi:10.1002/2014GB004951
- INMET-National Institute of Meteorology. 2023. INMET Meteorological Database. <https://bdmep.inmet.gov.br/>
- Iversen, N., and B. B. Jørgensen. 1985. Anaerobic methane oxidation rates at the sulfate-methane transition in marine sediments from Kattegat and Skagerrak (Denmark). *Limnol. Oceanogr.* **30**: 944–955.
- Jacotot, A., C. Marchand, and M. Allenbach. 2018. Tidal variability of CO₂ and CH₄ emissions from the water column within a Rhizophora mangrove forest (New Caledonia). *Sci. Total Environ.* **631–632**: 334–340. doi:10.1016/j.scitotenv.2018.03.006
- Jeffrey, L. C., D. T. Maher, I. R. Santos, M. Call, M. J. Reading, C. Holloway, and D. R. Tait. 2018. The spatial and temporal drivers of pCO₂, pCH₄ and gas transfer velocity within a subtropical estuary. *Estuar. Coast. Shelf Sci.* **208**: 83–95. doi:10.1016/j.ecss.2018.04.022
- Jeffrey, L. C., G. Reithmaier, J. Z. Sippo, S. G. Johnston, D. R. Tait, Y. Harada, and D. T. Maher. 2019. Are methane emissions from mangrove stems a cryptic carbon loss pathway? Insights from a catastrophic forest mortality. *New Phytol.* **224**: 146–154. doi:10.1111/nph.15995
- Jørgensen, B. B., A. Weber, and J. Zopfi. 2001. Sulfate reduction and anaerobic methane oxidation in Black Sea sediments. *Deep-Sea Res. I Oceanogr. Res. Pap.* **48**: 2097–2120. doi:10.1016/S0967-0637(01)00007-3
- Kristensen, E., M. Flindt, S. Ulomi, A. Borges, G. Abril, and S. Bouillon. 2008. Emission of CO₂ and CH₄ to the atmosphere by sediments and open waters in two Tanzanian mangrove forests. *Mar. Ecol. Prog. Ser.* **370**: 53–67. doi:10.3354/meps07642
- Kristensen, E., T. Valdemarsen, P. Moraes, A. Güth, P. Sumida, and C. Quintana. 2022. Pneumatophores and crab burrows increase CO₂ and CH₄ emission from sediments in two Brazilian fringe mangrove forests. *Mar. Ecol. Prog. Ser.* **698**: 29–39. doi:10.3354/meps14153

- Lan, X., K. W. Thoning, and E. J. Dlugokencky. 2023. Trends in globally-averaged CH₄, N₂O, and SF₆ determined from NOAA Global Monitoring Laboratory measurements. Version 2023-10. <https://doi.org/10.15138/P8XG-AA10>
- Le Mer, J., and P. Roger. 2001. Production, oxidation, emission and consumption of methane by soils: A review. *Eur. J. Soil Biol.* **37**: 25–50. doi:10.1016/S1164-5563(01)01067-6
- Lilley, M. D., M. A. De Angelis, and E. J. Olson. 1996. Methane concentrations and estimated fluxes from Pacific Northwest rivers. *Internationale Vereinigung Für Theoretische Und Angewandte Limnologie: Mitteilungen.* **25**(1): 187–196. doi:10.1080/05384680.1996.11904080
- Linto, N., J. Barnes, R. Ramachandran, J. Divia, P. Ramachandran, and R. C. Upstill-Goddard. 2014. Carbon dioxide and methane emissions from mangrove-associated waters of the Andaman Islands, Bay of Bengal. *Estuar. Coasts* **37**: 381–398. doi:10.1007/s12237-013-9674-4
- Lovelock, C. E., and others. 2022. Modeled approaches to estimating blue carbon accumulation with mangrove restoration to support a blue carbon accounting method for Australia. *Limnol. Oceanogr.* **67**: 50–60. doi:10.1002/lno.12014
- Maher, D. T., M. Call, I. R. Santos, and C. J. Sanders. 2018. Beyond burial: Lateral exchange is a significant atmospheric carbon sink in mangrove forests. *Biol. Lett.* **14**: 20180200. doi:10.1098/rsbl.2018.0200
- Mao, S.-H., and others. 2022. Aerobic oxidation of methane significantly reduces global diffusive methane emissions from shallow marine waters. *Nat. Commun.* **13**: 7309. doi:10.1038/s41467-022-35082-y
- MapBiomass Project. 2024. Annual Land Use and Land Cover Mapping of Brazil - Collection 8. <https://brasil.mapbiomas.org/en/>
- Neubauer, S. C., and J. P. Megonigal. 2015. Moving beyond global warming potentials to quantify the climatic role of ecosystems. *Ecosystems* **18**: 1000–1013. doi:10.1007/s10021-015-9879-4
- Pataki, D. E., and others. 2003. The application and interpretation of Keeling plots in terrestrial carbon cycle research. *Global Biogeochem. Cycles* **17**: 2001GB001850. doi:10.1029/2001GB001850
- R Core Team. 2021. R: Language and environment for statistical computing. In R Foundation for Statistical Computing. Vienna, Austria. <https://www.r-project.org/>
- Reeburgh, W. S. 2007. Oceanic methane biogeochemistry. *Chem. Rev.* **107**: 486–513. doi:10.1021/cr050362v
- Reithmaier, G. M. S., and others. 2023. Carbonate chemistry and carbon sequestration driven by inorganic carbon outwelling from mangroves and saltmarshes. *Nat. Commun.* **14**: 8196. doi:10.1038/s41467-023-44037-w
- Rosentreter, J., D. Maher, D. Ho, M. Call, J. Barr, and B. Eyre. 2017. Spatial and temporal variability of CO₂ and CH₄ gas transfer velocities and quantification of the CH₄ microbubble flux in mangrove dominated estuaries. *Limnol. Oceanogr.* **62**: 561–578. doi:10.1002/lno.10444
- Rosentreter, J. A., D. T. Maher, D. V. Erler, R. H. Murray, and B. D. Eyre. 2018. Methane emissions partially offset “blue carbon” burial in mangroves. *Sci. Adv.* **4**: eaao4985. doi:10.1126/sciadv.aao4985
- Rosentreter, J. A., A. N. Al-Haj, R. W. Fulweiler, and P. Williamson. 2021. Methane and nitrous oxide emissions complicate coastal blue carbon assessments. *Global Biogeochem. Cycles* **35**: 2. doi:10.1029/2020GB006858
- Rosentreter, J. A., and others. 2023. Coastal vegetation and estuaries are collectively a greenhouse gas sink. *Nat. Clim. Chang.* **13**: 579–587. doi:10.1038/s41558-023-01682-9
- Sánchez-Carrillo, S., J. Garatuza-Payan, R. Sánchez-Andrés, F. J. Cervantes, M. C. Bartolomé, M. Merino-Ibarra, and F. Thalasso. 2021. Methane production and oxidation in mangrove soils assessed by stable isotope mass balances. *Water* **13**: 1867. doi:10.3390/w13131867
- Santos, I. R., D. T. Maher, R. Larkin, J. R. Webb, and C. J. Sanders. 2019. Carbon outwelling and outgassing vs. burial in an estuarine tidal creek surrounded by mangrove and saltmarsh wetlands. *Limnol. Oceanogr.* **64**: 996–1013. doi:10.1002/lno.11090
- Sawakuchi, H. O., and others. 2016. Oxidative mitigation of aquatic methane emissions in large Amazonian rivers. *Glob. Change Biol.* **22**: 1075–1085. doi:10.1111/gcb.13169
- Schenk, J., and others. 2021. Methane in lakes: Variability in stable carbon isotopic composition and the potential importance of groundwater input. *Front. Earth Sci.* **9**: 722215. doi:10.3389/feart.2021.722215
- Segarra, K. E. A., F. Schubotz, V. Samarkin, M. Y. Yoshinaga, K.-U. Hinrichs, and S. B. Joye. 2015. High rates of anaerobic methane oxidation in freshwater wetlands reduce potential atmospheric methane emissions. *Nat. Commun.* **6**: 7477. doi:10.1038/ncomms8477
- Taketani, R. G., C. A. Yoshiura, A. C. F. Dias, F. D. Andreote, and S. M. Tsai. 2010. Diversity and identification of methanogenic archaea and sulphate-reducing bacteria in sediments from a pristine tropical mangrove. *Antonie Van Leeuwenhoek* **97**: 401–411. doi:10.1007/s10482-010-9422-8
- Tamborski, J. J., M. Eagle, B. L. Kurylyk, K. D. Kroeger, Z. A. Wang, P. Henderson, and M. A. Charette. 2021. Pore water exchange-driven inorganic carbon export from intertidal salt marshes. *Limnol. Oceanogr.* **9999**: 1–19. doi:10.1002/lno.11721
- Tyler, S. C., R. S. Bilek, R. L. Sass, and F. M. Fisher. 1997. Methane oxidation and pathways of production in a Texas paddy field deduced from measurements of flux, δ¹³C, and δD of CH₄. *Global Biogeochem. Cycles* **11**: 323–348. doi:10.1029/97GB01624
- Wang, F., P. Cheng, N. Chen, and Y. M. Kuo. 2020. Tidal driven nutrient exchange between mangroves and estuary reveals a dynamic source-sink pattern. *Chemosphere* **270**: 128665. doi:10.1016/j.chemosphere.2020.128665

- Wanninkhof, R. 2014. Relationship between wind speed and gas exchange over the ocean revisited. *Limnol. Oceanogr. Methods* **12**: 351–362. doi:[10.4319/lom.2014.12.351](https://doi.org/10.4319/lom.2014.12.351)
- Ward, N. D., T. S. Bianchi, J. B. Martin, C. J. Quintero, H. O. Sawakuchi, and M. J. Cohen. 2020. Pathways for methane emissions and oxidation that influence the net carbon balance of a subtropical cypress swamp. *Front. Earth Sci.* **8**: 573357. doi:[10.3389/feart.2020.573357](https://doi.org/10.3389/feart.2020.573357)
- Webb, J. R., D. T. Maher, and I. R. Santos. 2016. Automated, in situ measurements of dissolved CO₂, CH₄ and δ¹³C values using cavity enhanced laser absorption spectrometry: Comparing response times of air-water equilibrators: Equilibrator measurement of dissolved CO₂, CH₄, and δ¹³C values. *Limnol. Oceanogr. Methods* **14**: 323–337. doi:[10.1002/lom3.10092](https://doi.org/10.1002/lom3.10092)
- Weiss, R. F. 1974. Carbon dioxide in water and seawater: The solubility of a non-ideal gas. *Mar. Chem.* **2**: 203–215. doi:[10.1016/0304-4203\(74\)90015-2](https://doi.org/10.1016/0304-4203(74)90015-2)
- Whiticar, M. J. 1999. Carbon and hydrogen isotope systematics of bacterial formation and oxidation of methane. *Chem. Geol.* **161**: 291–314. doi:[10.1016/S0009-2541\(99\)00092-3](https://doi.org/10.1016/S0009-2541(99)00092-3)
- Xiao, K., and others. 2020. Large CO₂ release and tidal flushing in salt marsh crab burrows reduce the potential for blue carbon sequestration. *Limnol. Oceanogr.* **9999**: 1–16. doi:[10.1002/lno.11582](https://doi.org/10.1002/lno.11582)
- Xin, P., and others. 2022. Surface water and groundwater interactions in salt marshes and their impact on plant ecology and coastal biogeochemistry. *Rev. Geophys.* **60**: 1–54. doi:[10.1029/2021RG000740](https://doi.org/10.1029/2021RG000740)
- Yamamoto, S., J. B. Alcauskas, and T. E. Crozier. 1976. Solubility of methane in distilled water and seawater. *J. Chem. Eng. Data* **21**: 78–80. doi:[10.1021/je60068a029](https://doi.org/10.1021/je60068a029)
- Yau, Y. Y. Y., and others. 2022. Alkalinity export to the ocean is a major carbon sequestration mechanism in a macrotidal saltmarsh. *Limnol. Oceanogr.* **67**: lno.12155. doi:[10.1002/lno.12155](https://doi.org/10.1002/lno.12155)
- Yau, Y. Y. Y., and others. 2023. Methane emissions in seagrass meadows as a small offset to carbon sequestration. *J. Geophys. Res. Biogeosci.* **128**: e2022JG007295. doi:[10.1029/2022JG007295](https://doi.org/10.1029/2022JG007295)

Acknowledgments

This work was primarily supported by Swedish Research Council grants to IRS (2019-03930 and 2020-00457). Additional funding includes a Swedish Research Council grant to SB (2022-04710), and instrumentation funded by a grant from the Fonds National de la Recherche Scientifique (FNRS) (U.N005.21-40003538) to AVB. AVB is a Research Director at FNRS. LCCJr is a Postdoc of the CARBOSTORE project (BMBF-Germany; 0370875B). WM thanks a research grant from the Brazilian Research Council (CNPq). GA is funded by the INEE-CNRS France-Brazil International Research Project VELITROP. We thank students from Fluminense Federal University and Federal University of Santa Catarina for field and laboratory support.

Conflict of Interest

None declared.

Submitted 11 November 2023

Revised 14 March 2024

Accepted 07 July 2024

Associate Editor: Oscar Serrano